Electronic Supplementary Information – Atomic domain magnetic nanoalloys - interplay between molecular structure and temperature dependent magnetic and dielectric properties in manganese doped tin clusters

1 Quantum Chemistry

1.1 Geometry of the dianions Sn_N^{2-}

The minimum energy dianionic tin structures obtained by the GA approach resemble the corresponding structures found in related borates and Zintl phases up to N=12. In accord to Wade's rule, the dianionic species build *closo* structures. The lowest energy structures of Sn_9^{2-} is a tricapped trigonal prism of D_{3h} symmetry, Sn_{10}^{2-} has the lowest energy with D_{4d} symmetry, a bicapped square antiprism. In the case of Sn_{11}^{2-} the hollow cage structure is C_{2v} symmetric, while Sn_{12}^{2-} shows the known icosahedral symmetry I_h of the Stannaspherene [1,2] with a large hollow site. Up to N =14 we continued the global optimization of the cage structure. The genetic algorithm approach, however, generated in the case of bare Sn_{13}^{2-} and Sn_{14}^{2-} prolate minimum energy structures without a hollow site. Apparently the cages get too large to retain the hollow site and collapse. However, in both cases isomers with relative energies of 0.96 eV (N =13) and 0.16 eV (N =14) compared to the global minima have cage structures. Upon doping with Mn^{2+} and local relaxation the corresponding structures are lower in energy than the Mn doped clusters corresponding to the lowest energy dianionic structures. The charges on a sphere method resulted in a C_{2v} symmetric cage structure of Sn_{13}^{2-} that was also found by the GA. However, in the case of Sn_{14}^{2-} the D_{6d} symmetric structure found by this simple approach was not identified by the GA. It is very close, but slightly higher in energy (at LANL2/DZ level of theory) than the lowest energy hollow cage structure (T_h) found by the GA. Identification of identical molecular structures in GAs is an important issue and while more sophisticated methods are now implemented in other codes, [3] the GA used for this study only uses the energy as a criterion to identify identical structures. Structures with the same or slightly higher energy than the next lower lying isomer are removed from the population. The structures obtained from charges on a sphere converged to the corresponding minimum structure obtained in the GA approach upon local optimization with up to 12 atoms, giving hope to obtain promising start geometries also for larger clusters. The geometries obtained with N charges on a sphere converged with $N = 15$ at D_3, $N = 16$ at C_3, $N = 17$ at D_{5h} and $N = 18$ at D_{4d} symmetry. The geometries obtained by global optimization and by the charges on a sphere model are presented in Fig. 1.

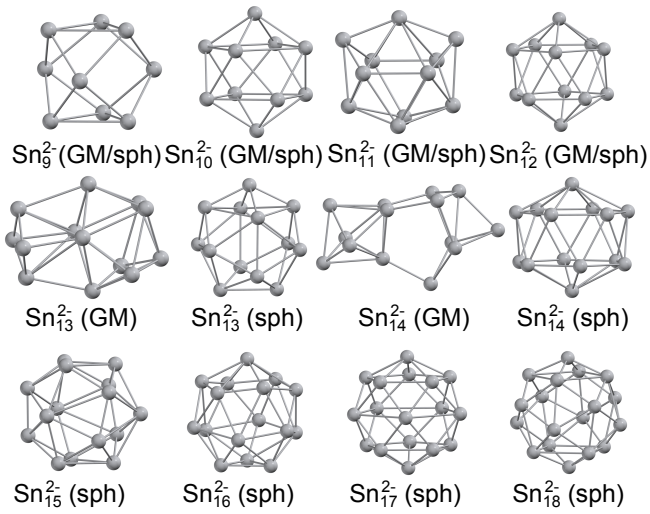

Fig. 1 Global minimum (GM) energy structures of the dianions Sn_N^{2-} and structures obtained by the charges on a sphere model (sph). The anionic structures with N = 9-12 are identical with both method (first line). With N = 13 and 14 the global minimum structures and those obtained by the spherical model differ (second line). With N = 15-18 only the structures generated by the charges on a sphere model are considered (third line).

1.2 Detailed geometric/dielectric data of Mn/Sn_N

In addition to the data presented in Fig. 1 of the main article, in Tab. 1 the components of the electric dipole moment and the moments of inertia of the Mn/Sn_N clusters are displayed, required for the molecular dynamics simulations of the dieletric response.

2 Mass spectrometry and fit procedure

Figure 2 shows a section of a TOF mass spectrum (MS) taken from one of the datasets. The MS presented was recorded close to the position of maximum intensity (z_0) and represents typical measurement conditions. Sn_N clusters can be observed with N = 10 – 18 and in between the corresponding signals of Mn/Sn_N with N = 9–18 are located. The mass of Mn is roughly half the mass of Sn, allowing to separate the signals for integration. However in the range of 12–19 Sn atoms, neighbouring signals overlap at the base, causing the

Table 1 Results of the DFT studies (Mn/Sn_N clusters). The first column contains the label of the cluster geometries of Mn/Sn_N as shown in Fig. 1 in the main article. $\Delta E_{B3P86,min}$ is the relative energy compared to the global minimum of the cluster isomer (minimum on the B3P86 PES), and $\Delta E_{BP86,SP}$ is the relative single point SCF energy in eV, obtained with the same geometry and the BP86 GGA functional. *Symm* denotes the point group symmetry and $M = 2S+1$ the spin multiplicity. μ_x, μ_y and μ_z are the components and $\mu_{el,0}$ the total magnitude of the permanent electric dipole moment in the molecular fixed frame in Debye, and α is the static polarizability in $Å^3$. I_x, I_y and I_z are the moments of inertia in the body fixed frame, given in 10^{-43} kg m^2.

Lable	$\Delta_{E,B3P86,min}$	$\Delta_{E,BP86,SP}$	*Symm*	*M*	μ_x	μ_y	μ_z	$\mu_{el,0}$	α	I_x	I_y	I_z
9.0.s	0.0000	0.0000	C_{3v}	6	0.00	0.00	-1.42	1.42	69.83	0.836	0.836	1.083
9.1.q	0.5208	0.2901	C_s	4	-0.34	0.00	-0.43	0.55	69.46	0.784	0.906	1.051
9.2.q	0.8664	0.4206	C_s	4	0.00	-0.53	-0.26	0.59	69.02	0.802	0.878	1.040
10.0.s	0.0000	0.1895	D_{4d}	6	0.00	0.00	0.00	0.00	74.24	0.956	1.091	1.091
10.1.q	0.0639	0.0000	C_{3v}	4	0.00	0.00	0.63	0.63	73.02	1.016	1.016	1.063
10.2.q	0.0650	0.0038	C_{2v}	4	0.00	0.00	0.67	0.67	72.98	1.004	1.026	1.064
11.0.q	0.0000	0.0000	C_{5v}	4	0.00	0.00	-0.26	0.26	79.38	1.197	1.197	1.326
11.1.s	0.4099	0.4903	C_s	6	0.00	0.23	0.51	0.56	80.40	1.141	1.282	1.322
11.2.q	0.6821	0.6050	C_{2v}	4	0.54	0.00	0.00	0.54	81.77	1.131	1.254	1.477
11.3.q	0.8234	0.6428	C_1	4	1.87	0.24	0.01	1.89	81.25	1.057	1.350	1.402
12.0.s	0.0000	0.0000	I_h	6	0.00	0.00	0.00	0.00	84.11	1.412	1.412	1.412
12.1.q	1.0010	0.7261	D_{5d}	4	0.00	0.00	0.00	0.00	83.94	1.375	1.375	1.455
12.2.s	2.1820	2.2258	C_{3v}	6	-4.42	0.00	0.00	4.42	91.70	1.436	1.487	1.487
13.0.s	0.0000	0.1753	C_s	6	1.14	0.51	0.00	1.25	94.73	1.398	1.863	1.881
13.1.q	0.0088	0.0000	C_s	4	-0.97	0.28	0.00	1.01	95.10	1.346	1.905	1.908
13.2.s	0.0258	0.1927	C_{2v}	6	-0.46	0.00	0.00	0.46	92.82	1.570	1.625	1.831
13.3.q	0.1111	0.1086	C_s	4	0.00	-0.05	-0.32	0.32	93.30	1.498	1.707	1.859
13.4.q	0.1147	0.1339	C_{2v}	4	-0.82	0.00	0.00	0.82	93.35	1.451	1.719	1.890
14.0.s	0.0000	0.0991	D_{6d}	6	0.00	0.00	0.00	0.00	98.61	1.799	1.799	2.096
14.1.q	0.1082	0.0000	C_1	4	-0.12	0.07	-0.22	0.26	99.52	1.670	1.940	2.144
14.2.s	0.1628	0.1985	T_h	6	0.00	0.00	0.00	0.00	98.94	1.873	1.873	1.873
14.3.d	0.3214	0.2020	C_{2v}	2	0.00	-0.10	0.00	0.10	100.06	1.666	1.969	2.139
15.0.s	0.0000	0.0424	C_s	6	0.32	0.00	0.28	0.42	105.62	1.992	2.199	2.219
15.1.q	0.0439	0.0000	C_2	4	0.00	0.00	-0.18	0.18	105.32	1.953	2.187	2.252
16.0.q	0.0000	0.0000	C_{3v}	4	-0.29	0.00	0.00	0.29	112.11	2.372	2.377	2.377
16.1.s	0.4041	0.4792	C_{3v}	6	0.00	0.00	-0.64	0.64	112.96	2.373	2.373	2.428
17.0.s	0.0000	0.0000	C_{5v}	6	-0.99	0.00	0.00	0.99	122.04	2.181	3.109	3.109
17.1.q	0.4285	0.2790	C_1	4	0.58	-1.30	-0.06	1.43	124.38	2.260	2.880	3.279
18.0.s	0.0000	0.0000	C_1	6	0.48	-0.34	-0.19	0.62	130.40	2.543	3.326	3.359
18.1.q	0.9043	0.5545	C_1	4	2.15	0.50	1.17	2.49	131.89	2.593	3.151	3.480

base line of the MS to deviate considerably from zero intensity (dotted black line). The signals of clusters containing tin naturally have wide mass distribution due to the large number of stable isotopes. With tin as primary component in the nanoalloys, broad signals are obtained. Simple numerical integration in the range between the corresponding minima causes the effect of the cluster species to be obscured by the effect on neighbouring signals. Therefore, a baseline correction is implemented to the analysis, based on Gaussian fits of the mass signals (see Fig. 2, red line). The measured data (black line) is reproduced very well by the red line obtained as the sum of one Gaussian for each cluster species. Initially, amplitude, variance and peak position of each Gaussian are fitted by least squares to the experimental MS with maximum intensity, i.e. with the scanning slit in the centre of the molecular beam (z_0). Except for a small correction of the peak positions, only the amplitude of each Gaussian function is then varied to obtain the fitted MS for every measured MS in the dataset. The molecular beam profiles are obtained as the analytic integrals of the mass signals as a function of the slit position.

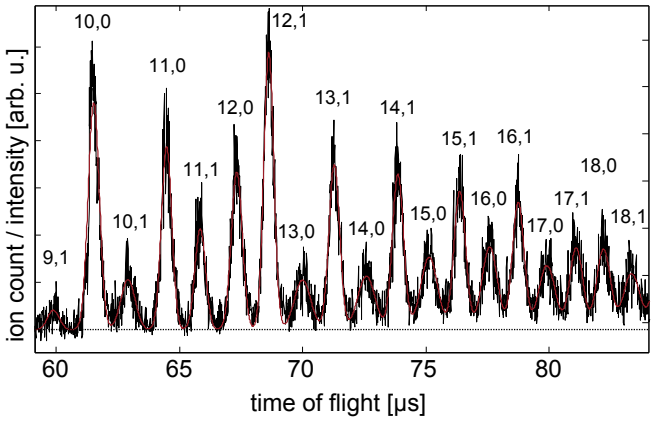

Fig. 2 Photo ionisation mass spectrum of Sn_N and Mn/Sn_N clusters. Signals of manganese doped clusters emerge in between the pure tin cluster signals. The peaks are labelled by $N,1$ and $N,0$ corresponding to the number on Sn and Mn atoms, respectively. Note the minute intensities of Mn/Sn_9 and $Mn@Sn_{10}$. Additionally the signals of the larger clusters are not very well separated. A least squares fit procedure to apply Gaussian functions to each signal in the range of interest was implemented, resembling the overlapping signals and hence correcting the baseline error (see text). The sum of all Gaussian functions is the smooth red line.

3 Vibrational temperature from magnetic response

The observed response of $Mn@Sn_{12}$ allows to obtain an experimental estimate of the vibrational temperature of the clusters in the molecular beam experiment. At very low nozzle temperatures the equilibration before expansion into vacuum is possibly insufficient and $T_{vib} > T_{nozzle}$.[4] We use the two-component model proposed in ref. [4] that describes the magnetic response of $Mn@Sn_{12}$ at any temperature to obtain T_{vib} from the simulation with least square error. We obtain 28, 34, 45 and 69 K for T_{vib} at T_{nozzle}= 16, 30, 50 and 70 K, respectively. The results agree with the assumption of $T_{vib} \approx T_{nozzle}$ at higher T_{nozzle}, taking into account an estimated uncertainty of $\pm$ 5 K, but indeed clearly show increasing deviations in the low temperature regime. We consequently use the value of T_{vib} that produces the best agreement of the two component model and the experimentally observed response of $Mn@Sn_{12}$ of each set of data to obtain the values of $\mu_{mag,0}$ plotted in Fig. 4 and P_0 values used in Fig. 5 of the main article.

Notes and references

1 L.-F. Cui, X. Huang, L.-M. Wang, D. Y. Zubarev, A. I. Boldyrev, J. Li and L.-S. Wang, *J. Am. Chem. Soc.*, 2006, **128**, 8390.

2 L.-F. Cui, X. Huang, L.-M. Wang, J. Li and L.-S. Wang, *Angew. Chemie*, 2007, **119**, 756.

3 S. Heiles and R. L. Johnston, *Int. J. Quantum Chem.*, 2013, **113**, 2091.

4 U. Rohrmann and R. Schäfer, *Phys. Rev. Lett.*, 2013, **111**, 133401.